



# Velocity crossover between hydrous and anhydrous forsterite at high pressures

Z. Mao <sup>a,\*</sup>, S.D. Jacobsen <sup>b</sup>, F. Jiang <sup>a</sup>, J.R. Smyth <sup>c</sup>, C.M. Holl <sup>a,b</sup>, D.J. Frost <sup>d</sup>, T.S. Duffy <sup>a</sup>

<sup>a</sup> Princeton University, Department of Geosciences, Princeton, NJ 08544, USA

<sup>b</sup> Northwestern University, Department of Earth and Planetary Sciences, Evanston, IL 60208, USA

<sup>c</sup> University of Colorado, Department of Geological Sciences, Boulder, CO 80309, USA

<sup>d</sup> Bayerisches Geoinstitut, Universität Bayreuth, Bayreuth 95440, Germany

## ARTICLE INFO

### Article history:

Received 14 May 2009

Received in revised form 30 December 2009

Accepted 16 February 2010

Available online 31 March 2010

Editor: L. Stixrude

### Keywords:

hydrous forsterite  
Brillouin scattering  
elasticity  
velocity crossover

## ABSTRACT

The elastic properties of hydrous forsterite,  $\text{Mg}_{2-x}\text{SiO}_4\text{H}_{2x}$ , are relevant to interpreting seismic velocity anomalies in the Earth's mantle. In this study, we used Brillouin scattering to determine the single-crystal elasticity of forsterite with 0.9(1) wt.%  $\text{H}_2\text{O}$  ( $x=0.14$ ) to 14 GPa. Aggregate bulk and shear moduli of hydrous forsterite increase with pressure at a greater rate than those of the corresponding anhydrous phase. Compared with anhydrous forsterite, we observe a 7% increase in the pressure derivative of the bulk modulus ( $K'_{50} = 4.50(5)$ ), and a 25% increase in the pressure derivative of the shear modulus ( $G'_0 = 1.75(5)$ ) for forsterite with near maximum possible water content. Using our results, we calculated the compressional,  $V_p$ , and shear,  $V_s$ , velocities of forsterite as a function of pressure at 300 K. Whereas  $V_p$  and  $V_s$  of hydrous forsterite are 0.6% and 0.4% slower than those of anhydrous forsterite at ambient pressure, velocity crossovers at  $\sim 3\text{--}4$  GPa result in higher hydrous forsterite velocities at pressures corresponding to depths below  $\sim 120$  km. At the pressure of the 410-km discontinuity,  $V_p$  and  $V_s$  of hydrous forsterite exceed those of anhydrous forsterite by 1.1(1)% and 1.9(1)%, respectively. This implies that incorporation of water could decrease the magnitude of the velocity contrast at 410-km depth between forsterite and wadsleyite. Although the effects of hydration on temperature derivatives of the elastic moduli of forsterite and wadsleyite are not yet known, from the current data we estimate that the presence of  $\sim 0.4$  wt.%  $\text{H}_2\text{O}$  in forsterite (at 60 mol%) could lower the P and S velocity contrast at 410-km depth to 3.8(4)% and 4.8(6)%, respectively. At high pressures, hydration also decreases the  $V_p/V_s$  ratio of forsterite, and lowers the maximum P wave azimuthal anisotropy and S wave splitting of forsterite.

© 2010 Elsevier B.V. All rights reserved.

## 1. Introduction

Hydrogen carried into the mantle via subduction could be incorporated into nominally anhydrous mantle minerals as hydroxyl defects (e.g. Smyth, 1987) with implications for water cycling in the Earth (e.g. Bercovici and Karato, 2003; Hirschmann, 2006; Jacobsen and van der Lee, 2006). A number of studies have examined the effect of hydrogen on various physical properties of mantle minerals, including melting (e.g. Inoue, 1994), rheology (e.g. Karato et al., 1986; Mei and Kohlstedt, 2000a,b) and electrical conductivity (Huang et al., 2005; Manthilake et al., 2009; Yoshino et al., 2008), etc. In this study, we focus on the elastic properties, which can also be affected by hydrogen defects (e.g. Jacobsen, 2006; Wang et al., 2006; Mao et al., 2008a; Tsuchiya and Tsuchiya, 2009).

Interpretation of seismic data requires knowledge of the elastic and anelastic properties of mantle minerals at high pressure and temperature. By comparing measured elastic properties and seismic results, we can potentially constrain mantle composition and

distinguish regions of hydrogen enrichment from regions of high temperature or partial melt.

Among the main mantle minerals, olivine and high-pressure polymorphs, wadsleyite and ringwoodite, are particularly important as these constitute  $\sim 60$  vol.% of a pyrolite model mantle. Olivine polymorphs can accommodate variable amounts of hydrogen into their structures (e.g. Smyth, 1987; Kohlstedt et al., 1996; Bolfan-Casanova et al., 2000; Demouchy et al., 2005). Even though olivine has the lowest hydrogen storage capacity among olivine polymorphs, it is still expected to incorporate a maximum of up to  $\sim 0.5$  wt.%  $\text{H}_2\text{O}$  at conditions along a mantle geotherm ( $\sim 1400$  °C at 12 GPa) (Hirschmann et al., 2005; Smyth et al., 2006; Mosenfelder et al., 2006; Hushur et al., 2009). Experimental and theoretical studies suggest that  $\text{Mg}^{2+}$  vacancies at the M1 octahedral sites are the main locations of hydration in forsterite (Brodholt, 1997; Churakov et al., 2003; Kudoh, 2008). From infrared spectroscopic studies, it is inferred that hydrogens locate along O–O octahedral edges (Smyth et al., 2006). However, the distribution and location of hydrogen in the structure may depend on a variety of factors including synthesis conditions, Fe content and oxidation state.

Previous studies showed that elastic properties of wadsleyite and ringwoodite are significantly decreased by the presence of hydrogen at ambient conditions (Inoue et al., 1998; Wang et al., 2003; Jacobsen,

\* Corresponding author. Now at The University of Texas at Austin, Department of Geological Sciences, Jackson School of Geosciences, Austin, TX 78712, USA.

E-mail address: [zhu.mao@jsg.utexas.edu](mailto:zhu.mao@jsg.utexas.edu) (Z. Mao).

2006; Mao et al., 2008a). Based on single-crystal elasticity studies, the addition of 1 wt.% H<sub>2</sub>O causes ~7–8% reductions in the bulk,  $K_{50}$ , and shear,  $G_0$ , moduli of Mg<sub>2</sub>SiO<sub>4</sub> wadsleyite (Mao et al., 2008a), and ~6–8% and ~11–14% reductions in  $K_{50}$  and  $G_0$  of (Mg,Fe)<sub>2</sub>SiO<sub>4</sub> ringwoodite (Inoue et al., 1998; Wang et al., 2003; Jacobsen et al., 2004). Structural vacancies associated with hydration can lead to expanded oxygen distances, weakened interatomic forces, and thus reduced elastic moduli.

Based on static compression studies (e.g. (Holl et al., 2008)), pressure derivatives of the isothermal bulk moduli of hydrous olivine polymorphs are variable but generally higher than anhydrous values. From single-crystal elasticity studies, the pressure derivatives of the bulk modulus,  $K'_0 = (\partial K_0 / \partial P)_{T_0}$ , and shear modulus,  $G'_0 = (\partial G_0 / \partial P)_{T_0}$ , of Fe-free wadsleyite were found to be unaffected by the presence of 0.8 wt.% H<sub>2</sub>O (Mao et al., 2008b), but  $G'_0$  of ringwoodite was slightly increased by an addition of 2.3 wt.% H<sub>2</sub>O from 1.5(1) (Li, 2003) to 1.7(1) (Wang et al., 2006). Furthermore, 1 wt.% H<sub>2</sub>O in (Mg<sub>0.9</sub>Fe<sub>0.1</sub>)<sub>2</sub>SiO<sub>4</sub> ringwoodite was found to markedly increase  $K'_0$  from 4.1(2) to 5.3(4), and  $G'_0$  from 1.3(1) to 2.0(1) (Sinogeikin et al., 2001; Jacobsen and Smyth, 2006). The higher derivatives result in  $K'_5$  of hydrous ringwoodite becoming indistinguishable from that of anhydrous ringwoodite at ~12 GPa. Extrapolation to higher pressures at 300 K suggests a potential crossover at ~16 GPa whereby  $V_p$  of the hydrous phase would exceed that of anhydrous Fe-bearing ringwoodite (Jacobsen and Smyth, 2006). The nature and distribution of vacancies for a given structure may affect pressure derivatives of elastic moduli. Despite lower initial values, some elastic moduli may stiffen more rapidly with compression due, for example, to strong O–O repulsion associated with vacant sites.

Calculations under Earth's transition zone conditions indicate that acoustic velocities of Fe-free hydrous wadsleyite will be lower than those of the corresponding anhydrous phase (Mao et al., 2008b). Hydration of mantle wadsleyite thus has the potential to explain low shear anomalies from seismic observations of the transition zone (e.g. (Nolet and Zielhuis, 1994)). For ringwoodite, the hydrous phase was found to have a lower shear velocity but similar or greater compressional velocity than the anhydrous phase at close to transition zone pressures (Jacobsen and Smyth, 2006). The discordance between the compressional and shear velocities of hydrous ringwoodite was recently applied to explain velocity anomalies deep in the transition zone beneath central Tibet (Tseng and Chen, 2008).

Compared with wadsleyite and ringwoodite, the elastic properties of olivine are only weakly affected by the presence of hydrogen at ambient conditions. The incorporation of 0.9 wt.% H<sub>2</sub>O in forsterite, Mg<sub>2</sub>SiO<sub>4</sub>, causes only a 0.6% and 0.4% reductions in the compressional and shear velocities, respectively (Jacobsen et al., 2008, 2009). Hydration of upper mantle phases, especially olivine, has been frequently invoked to explain observed velocity anomalies (e.g. Vinnik and Farra, 2007; van der Lee et al., 2008) or uplift and broadening of the 410-km discontinuity (e.g. van der Meijde et al., 2003; Song et al., 2004). However, due to lack of experimental constraints on  $K'_{50}$  and  $G'_0$ , effects of hydration on the sound velocities of olivine at Earth's mantle conditions are still poorly known.

In this study, we report measurements of the single-crystal elasticity of forsterite with 0.9 wt.% H<sub>2</sub>O to 14 GPa by Brillouin scattering. Studies of the elasticity of Fe-free hydrous phases are useful because they allow separation of the effect of water from that of iron. Using the determined elastic tensor, we obtain the aggregate bulk and shear moduli at each pressure, and constrain their pressure derivatives. The results are applied to evaluate the effect of hydration on seismic images of the upper mantle, the magnitude of the velocity change at 410-km depth, and the anisotropy of forsterite at high pressures.

## 2. Experimental details

Single crystals of hydrous forsterite were synthesized in the 5000-ton multianvil press at Bayerisches Geoinstitut. The samples (run SZ0408A,

(Smyth et al., 2006) were the same ones used in a previous Brillouin study at ambient conditions (Jacobsen et al., 2008, 2009). The H<sub>2</sub>O content was determined by FTIR spectroscopy using the results of Bell et al. (2003). Determinations of H<sub>2</sub>O content for our samples require considerable extrapolation of the (Bell et al., 2003) calibration. We assign a nominal uncertainty of ~10%, and note that improved calibration for higher H<sub>2</sub>O contents is needed. Detailed information about the sample synthesis, including IR spectra, is reported by Smyth et al. (2006).

Three platelets of varying crystal orientation were double-side polished to ~40 μm thickness. Raman spectra were measured for each platelet over spectral ranges from 200 cm<sup>-1</sup> to 1200 cm<sup>-1</sup> and from 3000 cm<sup>-1</sup> to 4000 cm<sup>-1</sup> to confirm their identity (Fig. S1 and Table S1). The lattice modes are in generally good agreement with data for anhydrous forsterite (Chopelas, 1991) with a slight increase in the frequencies due to hydration (Table S1). The lattice modes of Fe-bearing anhydrous olivine have slightly lower frequency than hydrous and anhydrous Mg<sub>2</sub>SiO<sub>4</sub> (Table S1) (Kleppe and Jephcoat, 2006). The Raman spectra show broad OH modes occurring over the range 3475 cm<sup>-1</sup> to 3614 cm<sup>-1</sup> which are similar to the range of the major IR peaks in these samples (Smyth et al., 2006), and are consistent with observed OH modes for hydrous olivine ((Mg<sub>0.97</sub>Fe<sub>0.03</sub>)<sub>2</sub>SiO<sub>4</sub>) (Kleppe and Jephcoat, 2006).

Each platelet was loaded in a diamond anvil cell. Steel gaskets with a 250-μm hole pre-indented to 60 to 70 μm thickness were placed between the diamonds. A 16:3:1 methanol-ethanol-water mixture was used as a pressure medium. This liquid composition is known to remain hydrostatic to 10.5 GPa (Angel et al., 2007). Ruby was used for pressure determination. Three to four small ruby spheres were loaded inside the gasket hole and distributed around the sample platelet. Below 10.5 GPa, there were no detectable difference in the pressure obtained from different ruby spheres. Above 10.5 GPa, the difference was within 0.1 GPa. Because several of our datapoints were measured at pressures above the liquid-glass phase transition of the pressure medium, in the results (Section 3) we scrutinize the possible effect of non-hydrostaticity.

For each platelet, Brillouin spectra were recorded at 10° steps over a 180° range at 6 pressures up to 14 GPa. All Brillouin spectra were measured in a symmetric forward geometry with a 70° scattering angle. A solid state laser with a power of 150 mW and wavelength of 532.15 nm was used to excite the sample. Acoustic velocities,  $v$ , were obtained from the measured Brillouin frequency shift,  $\Delta\nu_B$ , by:

$$v = \frac{\Delta\nu_B \lambda_0}{2 \sin(\theta/2)}, \quad (1)$$

where  $\lambda_0$  is the incident wavelength and  $\theta$  is the external scattering angle. Fig. 1 shows an example of measured acoustic velocity data. As many as three acoustic modes, one quasi-longitudinal and two quasi-transverse, were observed in some directions. Sinogeikin and Bass (2000) estimate that error sources in the scattering geometry in the diamond anvil cell result in 0.5–1% limits on the precision of the recovered acoustic velocities. For the present study, the precision of repeated measurements in the same direction is within ±0.2% for the shear velocity, and ±0.5% for the compressional velocity. The greater error in compressional velocity is due to lower signal-to-noise ratio. Further experimental details can be found in Speziale and Duffy (2002).

## 3. Results

Christoffel's equation describes the relationship between elastic constants,  $C_{ij}$ , acoustic velocities,  $v$ , and the direction cosines,  $n_i$ , of the phonon propagation direction:

$$\det |C_{ijkl}n_jn_l - \rho v^2 \delta_{ik}| = 0, \quad (2)$$

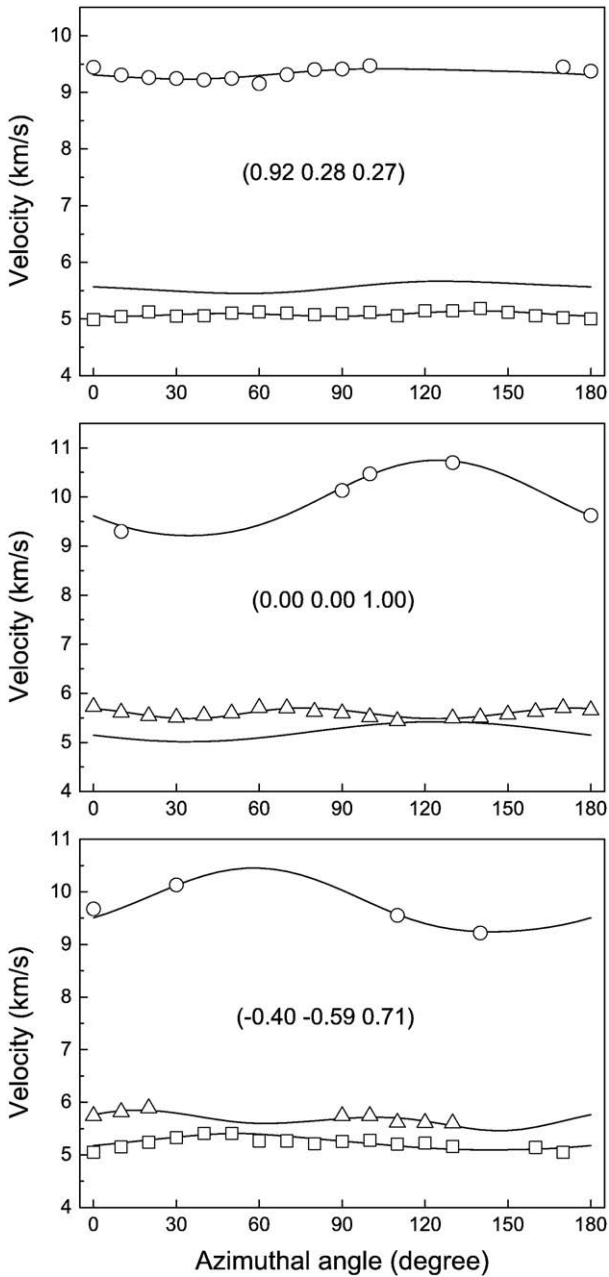


**Fig. 1.** Acoustic velocities of hydrous forsterite at 14.1 GPa. Open symbols are measurements; circle: P wave velocity; triangle: fast S wave velocity; square: slow S wave velocity; solid lines: fitting results. The crystallographic orientation of each platelet is indicated. Root-mean-square difference between calculated and measured velocities is 53 m/s.

where  $\rho$  is the density and the  $C_{ijkl}$  are the elastic constants in full suffix notation. Direction cosines,  $n_i$ , are determined from the Eulerian angles ( $\theta, \phi, \chi$ ) which relate the laboratory coordinate system to the crystal coordinate system (Shimizu, 1995). For each platelet, the Eulerian angles were determined by single-crystal X-ray diffraction at the X17C beamline of the National Synchrotron Light Source or in the Mineral Structures Laboratory at the University of Colorado. Non-linear least-squares inversion was used (Every, 1980) to fit velocity curves of all platelets to obtain the elastic constants and the orientations at each pressure (Fig. 1). The density at ambient conditions was calculated from measured unit cell volume and water content (Table 1) (Smyth et al., 2006; Jacobsen et al., 2008, 2009). At high pressures, densities were determined self-consistently

from the Brillouin data following the procedure described by Speziale and Duffy (2002).

Forsterite belongs to the orthorhombic crystal system and is thus characterized by 9 non-zero, independent elastic constants. Fig. 2 (Fig. S2) shows individual  $C_{ij}$  as a function of pressure compared with those of anhydrous forsterite (Zha et al., 1996). The data were fitted to third-order Eulerian finite strain equations to obtain the pressure derivative of each  $C_{ij}$  (Table 2). The longitudinal moduli  $C_{11}$  and  $C_{33}$ , shear modulus  $C_{44}$ , and off-diagonal moduli  $C_{12}$ ,  $C_{13}$  and  $C_{23}$ , follow similar trends as the anhydrous phase with pressure. Pressure derivatives of these six elastic constants are indistinguishable within uncertainties from those of the anhydrous phase. Longitudinal modulus,  $C_{22}$ , and shear moduli  $C_{55}$  and  $C_{66}$  increase faster with pressure in hydrous forsterite. In percentage terms, hydration most strongly affects the pressure derivatives of  $C_{22}$  (24% larger),  $C_{55}$  (27% larger), and  $C_{66}$  (17% larger) while all other pressure derivatives are within 10% of anhydrous values. The shear modulus,  $C_{55}$ , is 1.6% lower than its anhydrous value at ambient conditions (Jacobsen et al., 2008, 2009), but becomes 4.3% greater at 14.1 GPa. In addition,  $C_{22}$  of hydrous forsterite is  $\sim 4.5\%$  greater than that of anhydrous forsterite, and  $C_{66}$  are  $\sim 1.5\%$  greater at this pressure. Considering average values of the pressure derivatives of the longitudinal,  $\overline{C'_{11}} = (C'_{11} + C'_{22} + C'_{33})/3$ , shear,  $\overline{C'_{44}} = (C'_{44} + C'_{55} + C'_{66})/3$ , and off-diagonal moduli,  $\overline{C'_{12}} = (C'_{12} + C'_{13} + C'_{23})/3$ , we find that the pressure derivatives of  $\overline{C'_{11}}$  and  $\overline{C'_{44}}$  are greater for hydrous forsterite than anhydrous  $fo_{100}$  or  $fo_{90}$ , but that mean values of the pressure derivatives of the off-diagonal moduli are similar in hydrous and anhydrous forsterite. Similar results were found for hydrous wadsleyite (Mao et al., 2008b), but in this case, the increase in the mean pressure derivatives of the longitudinal modulus of wadsleyite with hydration is smaller than observed in forsterite.

From the individual  $C_{ij}$ s, we calculated the aggregate bulk and shear moduli using the VRH (Voigt–Reuss–Hill) average (Table 1 and Fig. 3). At ambient conditions, the presence of 0.9 wt.%  $H_2O$  causes a 2.7% reduction in the bulk modulus,  $K_S$ , and a 2.2% reduction in the shear modulus,  $G$  (Jacobsen et al., 2008, 2009). The difference in bulk moduli between hydrous and anhydrous forsterite decreases with increasing pressure. At 14.1 GPa, the bulk modulus of hydrous forsterite is indistinguishable from that of the anhydrous phase within uncertainty. Fitting the aggregate bulk modulus of hydrous forsterite to a third-order Eulerian finite strain equations yields  $K'_{S0} = 4.50(5)$ . Compared with anhydrous forsterite, hydration slightly increases  $K'_{S0}$  (Zha et al., 1996). Table 3 compares the  $K'_{S0}$  of olivine for different compositions. The addition of 0.9 wt.%  $H_2O$  affects this pressure derivative by an amount comparable to an addition of 10 to 15 mol% iron in olivine. A recent theoretical study (Liu et al., 2009) on the elasticity of hydrous forsterite using first-principle methods also finds that hydration would slightly increase  $K'_{S0}$  of forsterite.

The effect of hydration on  $G'_0$  of forsterite is more pronounced, and this also agrees with the first-principles calculation results (Liu et al., 2009). Beyond  $\sim 6$  GPa, the shear modulus of hydrous forsterite exceeds that of anhydrous forsterite (Fig. 3). At 14.1 GPa, the shear modulus of hydrous forsterite is 2.5% greater than that of anhydrous forsterite. Using third-order Eulerian finite strain equations, we obtained a pressure derivative of the shear modulus  $G'_0 = 1.75(5)$  for the hydrous phase, considerably greater than that of anhydrous forsterite ( $G'_0 = 1.4(1)$ ). Addition of 0.9 wt.%  $H_2O$  has a much greater effect on  $G'_0$  than an addition of 10 mol% of iron, and yields a  $G'_0$  value comparable to that for the Fe endmember fayalite (Table 3).

In order to evaluate the possible influence of non-hydrostatic stress on our results due to the solid pressure medium above 10.5 GPa, we fitted the variation of  $K$  and  $G$  with pressure using only the subset of our data below 10 GPa and compared with the fit to all the data. The resulting  $K'_{S0}$  and  $G'_0$  from the  $< 10$  GPa subset overlaps with the whole dataset trend within two standard deviations or less.

**Table 1**  
Single-crystal and aggregate elastic moduli of hydrous forsterite at high pressures.

$P$ (GPa)	$\rho$ (g/cm <sup>3</sup> )	$C_{11}$ (GPa)	$C_{22}$ (GPa)	$C_{33}$ (GPa)	$C_{44}$ (GPa)	$C_{55}$ (GPa)	$C_{66}$ (GPa)	$C_{12}$ (GPa)	$C_{13}$ (GPa)	$C_{23}$ (GPa)	$K_S$ (GPa)	$G$ (GPa)
0.0001	3.180(3)	314.4(6)	194.6(5)	233.7(7)	65.8(3)	79.9(2)	78.4(4)	64.7(6)	67.0(6)	70.0(6)	125.4(2)	79.6(1)
3.0	3.253(3)	329(3)	217(3)	252(3)	71(3)	83.2(13)	85.8(12)	72(2)	79(3)	78(5)	137.7(11)	84.8(8)
6.6	3.334(3)	355(4)	236(3)	261(4)	77.4(9)	91(1)	92.6(9)	85(3)	91(5)	95(2)	153.0(11)	89.7(8)
8.5	3.374(3)	379(5)	244(3)	268(4)	80.0(9)	94.7(13)	96.2(10)	94(3)	94(3)	97(2)	159.9(9)	93.2(9)
10.7	3.419(3)	388(5)	263(3)	295(5)	83.3(9)	100.1(10)	100.4(10)	102(4)	100(7)	110(3)	172.7(12)	97.7(6)
11.9	3.443(3)	390(4)	266(4)	304(5)	85.9(9)	100.9(10)	101.7(10)	105(4)	100(5)	112(3)	175.6(12)	99.2(6)
14.1	3.485(3)	403(4)	296(4)	307(5)	87.6(10)	102.5(10)	104.8(10)	117(4)	108(4)	120(3)	187.2(12)	102.0(4)

1 bar data are from Jacobsen et al. (2008, 2009).

$K_S$  and  $G$  are Voigt–Reuss–Hill averages.

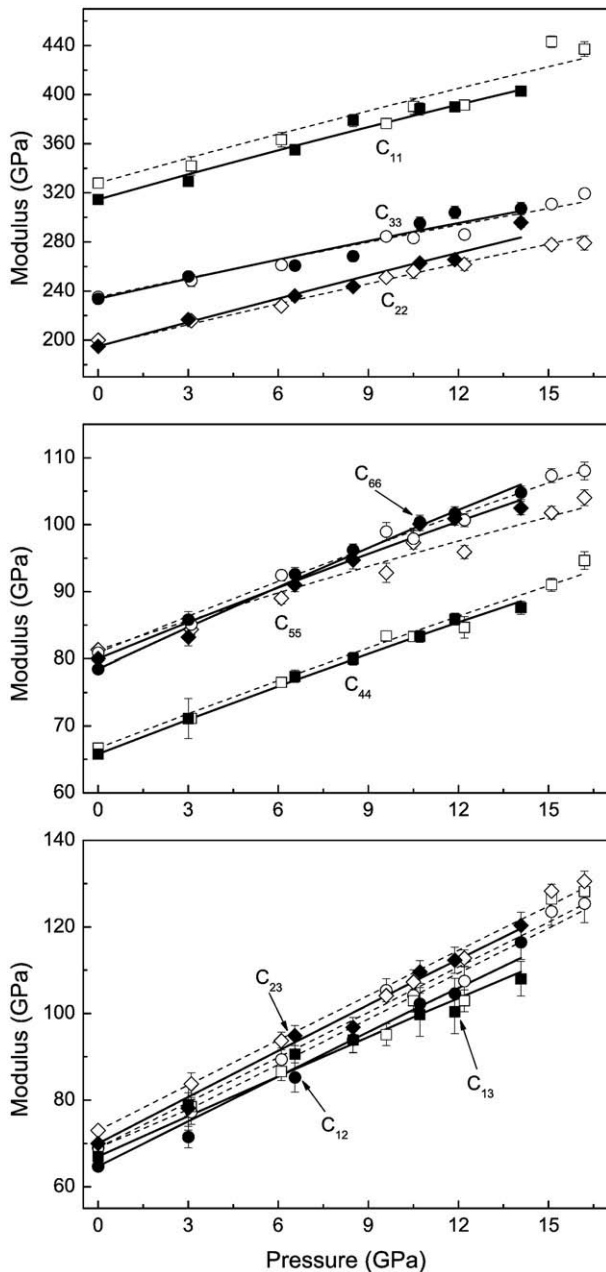


**Fig. 2.** Single-crystal elastic moduli of hydrous forsterite as a function of pressure. Solid symbols and lines: 0.9 wt.% H<sub>2</sub>O, hydrous forsterite ( $f_{0.100}$ ), this study; open symbols and dashed lines: anhydrous forsterite (Zha et al., 1996).

## 4. Discussion

### 4.1. Effect of hydration on elastic wave velocities of forsterite

Using our new data, we investigate the effect of hydration on aggregate sound velocities of forsterite with depth. We assume the elasticity of forsterite varies linearly with H<sub>2</sub>O content at ambient conditions (Jacobsen et al., 2008, 2009). Also, we assume a linear relationship between H<sub>2</sub>O content and the pressure derivatives of the bulk and shear moduli. Compressional and shear velocities are computed using third-order finite strain theory. Since the effect of temperature on the elasticity of hydrous olivine polymorphs is currently not available, all the calculations below were performed at 300 K.

Fig. 4 shows the calculated P and S wave velocities of forsterite with 0.9 wt.% H<sub>2</sub>O compared with dry conditions at 300 K. At 1-bar pressure, the compressional ( $V_P$ ), bulk ( $V_B$ ), and shear ( $V_S$ ) velocities of hydrous forsterite are slower than velocities in the anhydrous phase by 0.6%, 0.7% and 0.4% respectively (Fig. 5) (Jacobsen et al., 2008, 2009). Because of the larger pressure derivatives of  $K_S$  and  $G$ , aggregate sound velocities of hydrous forsterite increase more rapidly with pressure than anhydrous forsterite. The velocity of the hydrous phase crosses and exceeds that of the anhydrous phase occurs at about 4 GPa for  $V_P$ , and 3 GPa for  $V_S$ . This velocity crossover corresponds to depths in the Earth of ~120 km, and 90 km, respectively. Due to the small effects of hydrogen on  $K_{S0}$ , the difference in  $V_B$  between hydrous and anhydrous forsterite is within the uncertainty of the calculation over the whole pressure range. For  $V_P$  and  $V_S$ , the velocities of the hydrous phase are 1.1(1)% and 1.9(1)% faster than those of the anhydrous phase at 13.7 GPa (410-km depth) (Fig. 5), respectively. The presence of 0.9 wt.% H<sub>2</sub>O in forsterite increases the compressional velocity gradient from 0.0021(3) s<sup>-1</sup> to 0.0025(2) s<sup>-1</sup> from 200 to 400-km depth, and the shear velocity gradient from 0.0006(3) s<sup>-1</sup> to 0.0010(1) s<sup>-1</sup>.

In the Earth's mantle, the maximum water storage capacity will vary with depth but is expected to be generally lower than the H<sub>2</sub>O content in our samples. The variation of the maximum water storage capacity of olivine with depth was estimated in previous experimental

**Table 2**  
Pressure derivatives of individual  $C_{ij}$  of hydrous forsterite.

$C'_{ij}$	This study	Anhydrous $f_{0.100}$ <sup>a</sup>	Anhydrous $f_{0.90}$ <sup>b</sup>
$C'_{11}$	7.0(2)	6.7(2)	6.54
$C'_{22}$	6.7(1)	5.4(1)	5.38
$C'_{33}$	5.5(5)	5.2(1)	5.51
$C'_{44}$	1.8(1)	1.7(1)	1.67
$C'_{55}$	1.9(1)	1.5(1)	1.81
$C''_{55}$			-0.070
$C'_{66}$	2.1(1)	1.8(1)	1.93
$C'_{12}$	3.5(1)	3.7(1)	3.86
$C'_{13}$	3.1(2)	3.4(1)	3.57
$C'_{23}$	3.6(1)	3.5(1)	3.37

<sup>a</sup>  $f_{0.100}$ : forsterite, Mg<sub>2</sub>SiO<sub>4</sub> (Zha et al., 1996).

<sup>b</sup>  $f_{0.90}$ : olivine, (Mg<sub>0.9</sub>Fe<sub>0.1</sub>)<sub>2</sub>SiO<sub>4</sub> (Abramson et al., 1997).

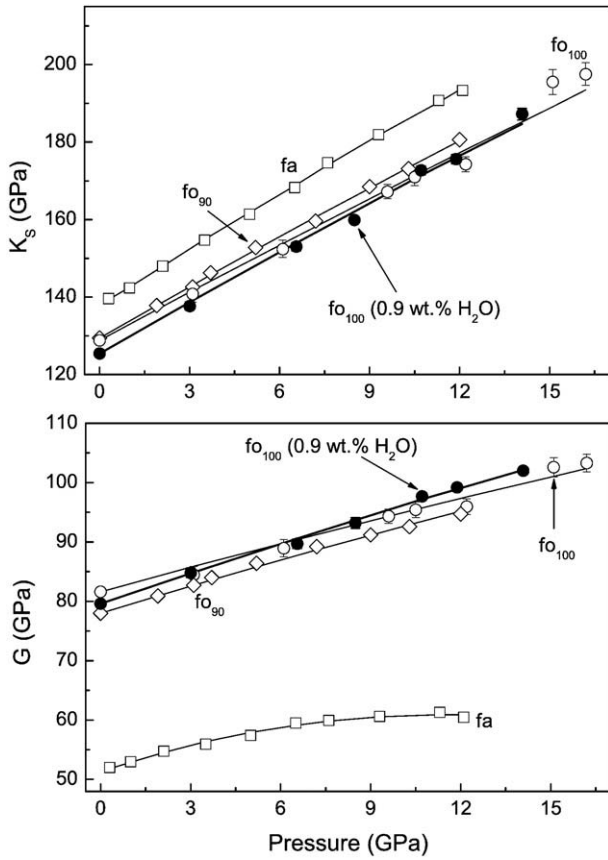


**Fig. 3.** Aggregate elastic moduli of forsterite as a function of pressure. Solid circle: hydrous forsterite ( $fo_{100}$ ,  $Mg_2SiO_4$ ), this study; open circle: anhydrous forsterite (Zha et al., 1996); diamond: Fe-bearing anhydrous forsterite ( $fo_{90}$ ,  $(Mg_{0.9}Fe_{0.1})_2SiO_4$ ) (Abramson et al., 1997); square: fayalite (fa,  $Fe_2SiO_4$ ) (Speziale et al., 2004).

studies (Hauri et al., 2006; Mosenfelder et al., 2006). In the study of Hauri et al. (2006),  $H_2O$  contents in olivine coexisting with melt were determined at various  $P$ - $T$  conditions using Secondary Ion Mass Spectroscopy on quenched samples. The  $H_2O$  storage capacity of olivine along the  $H_2O$ -saturated solidus was found to be low near ambient but increased steadily with pressure eventually reaching a value of 0.9 wt.% at 13 GPa. Aggregate sound velocities calculated using this variable water content with depth are also shown in Figs. 4 and 5 for comparison. In this case, the velocities of hydrous olivine become steadily faster than those of anhydrous olivine below 200-km depth because of the combined effects of the higher elastic properties of the hydrous phase and the increased  $H_2O$  storage capacity of olivine with depth.

When interpreting seismic profiles and images, the effects of anelasticity may also need to be accounted for (Karato, 1993; Jackson

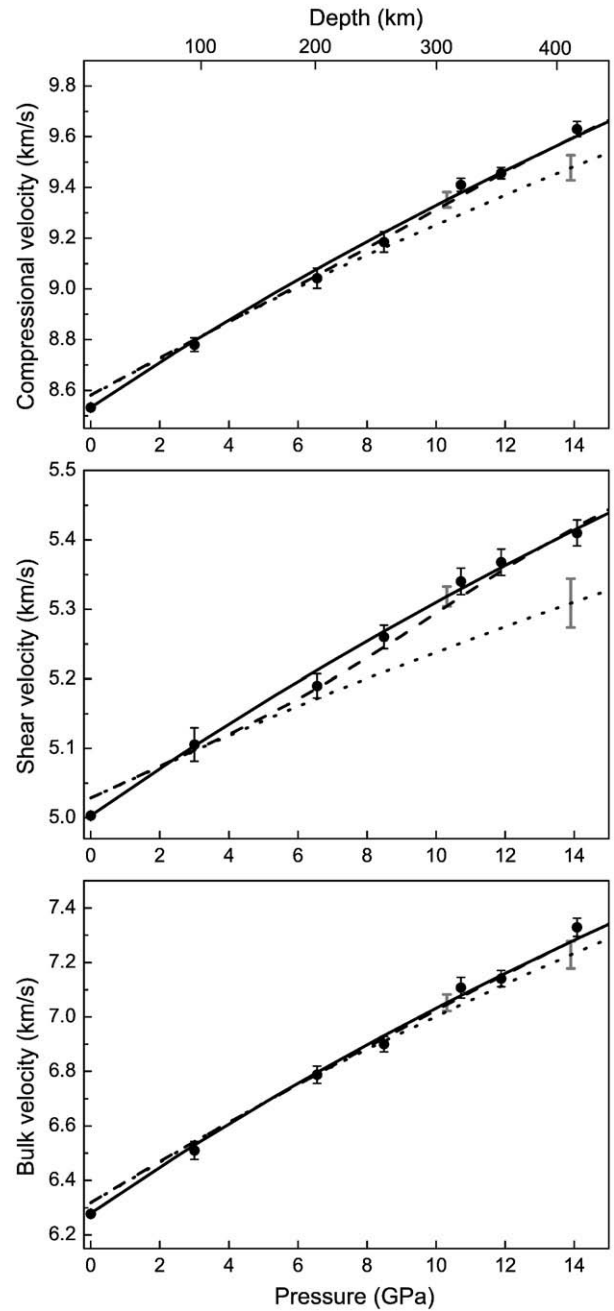


**Fig. 4.** Aggregate compressional, shear and bulk sound velocity of forsterite as a function of pressure at 300 K. Solid symbols: measured data for forsterite with 0.9 wt.%  $H_2O$ ; dotted line: dry; dashed line:  $H_2O$  varies with pressure according to Hauri et al. (2006). Representative uncertainties ( $1\sigma$ ) are shown. Depths along top axis are obtained from Earth model PREM (Dziewonski and Anderson, 1981).

**Table 3**

Pressure derivatives of the aggregate bulk and shear moduli for compositions along forsterite–fayalite join.

Ref.	Composition	$K'_{S0}$	$G'_0$
This study	$fo_{100}^a$ (0.9 wt.% $H_2O$ )	4.50(5)	1.75(5)
Zha et al. (1996)	$fo_{100}$	4.2(2)	1.4(1)
Abramson et al. (1997)	$fo_{90}^b$	4.4(1)	1.5(1) <sup>c</sup>
Speziale et al. (2004)	$fo_0^d$	4.9(1)	1.8(1) <sup>e</sup>

<sup>a</sup>  $fo_{100}$ : forsterite,  $Mg_2SiO_4$ .

<sup>b</sup>  $fo_{90}$ : olivine,  $(Mg_{0.9}Fe_{0.1})_2SiO_4$ .

<sup>c</sup> Refit using third-order Eulerian strain equation of state.

<sup>d</sup>  $fo_0$ : fayalite,  $Fe_2SiO_4$ .

<sup>e</sup>  $G'_0$  is  $-0.11(1) \text{ GPa}^{-1}$ .

et al., 2002). Hydrogen may enhance anelasticity (Karato, 1995; Aizawa et al., 2008) and lead to a reduction in the sound velocities of olivine. This may offset the increase in the anharmonic component velocity for hydrous forsterite observed here. Further examination of the elastic and anelastic properties of hydrous phases at mantle  $P$ - $T$  conditions and  $H_2O$  contents will be addressed in a later publication.

#### 4.2. $V_P/V_S$ ratio of hydrous forsterite

The  $V_P/V_S$  ratio is commonly used to identify compositional variations in the Earth's mantle. Here, we investigate the effect of hydration on the  $V_P/V_S$  ratio of forsterite (Fig. 6). The calculation,

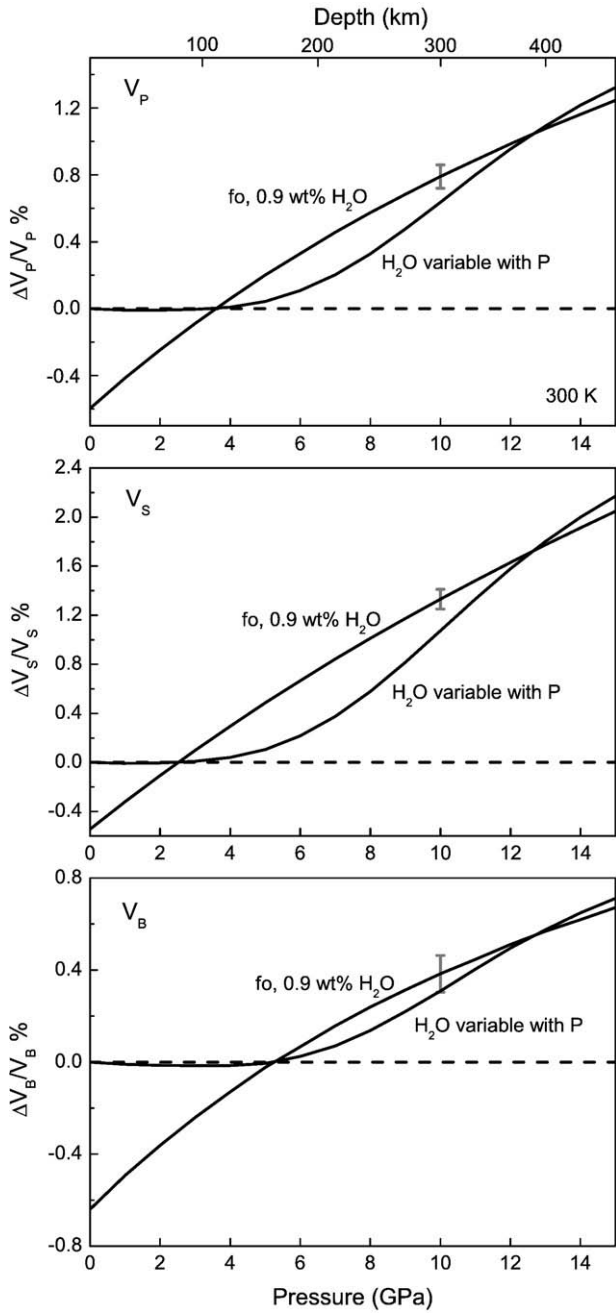


**Fig. 5.** Velocity change of forsterite caused by hydration relative to dry forsterite with pressure.  $\Delta V_X/V_X$  is  $(V_X^{H_2O} - V_X^{dry})/V_X^{dry}$ , where  $X$  is  $P$ ,  $S$  or  $B$  for compressional, shear and bulk velocity, respectively. Dashed line is for 0 reference. fo, 0.9 wt.%  $H_2O$ : hydrous forsterite containing 0.9 wt.%  $H_2O$ , and the constant water content with pressure;  $H_2O$  variable with  $P$ : water content in forsterite varies with pressure according to (Hauri et al., 2006). Representative uncertainties ( $1\sigma$ ) are shown.

following the method outlined in Section 4.1, is carried out for 300 K conditions, but it should be noted that temperature may also affect the  $V_p/V_s$  ratio (Isaak et al., 1989; Sinogeikin et al., 2003).

At ambient pressure, the  $V_p/V_s$  ratios of hydrous and anhydrous forsterite are almost the same,  $\sim 1.706(5)$ . With pressure,  $V_p/V_s$  weakly increases. At pressure corresponding to 410-km depth, the  $V_p/V_s$  of hydrous forsterite is increased to 1.770(6) compared to 1.783(6) for the anhydrous phase, a difference of 0.7%. A similar decrease in the  $V_p/V_s$  ratios caused by hydration was observed for ringwoodite (Wang et al., 2006). This contrasts with the behavior of Fe-bearing ringwoodite for which a 2.3% increase in  $V_p/V_s$  was observed in the hydrous phase

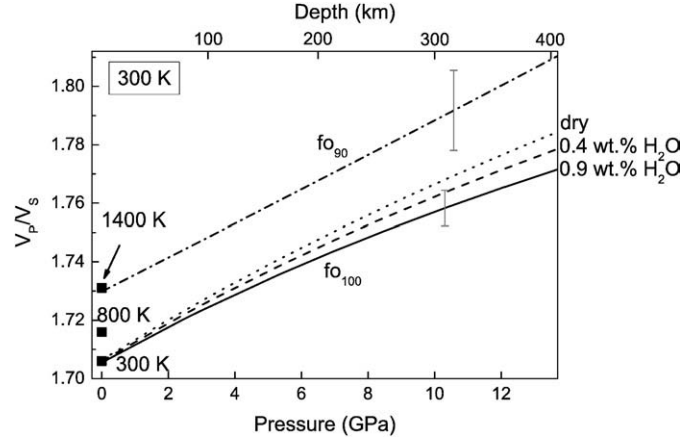


**Fig. 6.** The  $V_p/V_s$  ratio of forsterite with varying hydrogen content at ambient temperature. Dotted line: anhydrous (Zha et al., 1996); dashed line: 0.4 wt.%  $H_2O$ ; solid line: 0.9 wt.%  $H_2O$ ; dot-dashed line: anhydrous  $fo_{90}$  (Abramson et al., 1997); squares:  $fo_{100}$  at 300 K, 800 K and 1400 K (Isaak et al., 1989). Representative uncertainties ( $1\sigma$ ) are shown.

relative to anhydrous ringwoodite (Jacobsen and Smyth, 2006; Sinogeikin et al., 2003).

Increasing temperature or addition of iron will increase the  $V_p/V_s$  ratio of forsterite. Variation of 100 K in temperature or 10 mol% iron would cause a 0.12% or a 1.4% increase in the  $V_p/V_s$  ratio, respectively. Thus, the effect of 0.9 wt.%  $H_2O$  on the  $V_p/V_s$  ratio of forsterite at pressures corresponding to 410-km depth is equivalent to a  $\sim 600$  K temperature reduction or a 5 mol% reduction in Fe content.

#### 4.3. Effect of water on the velocity contrast at 410-km depth

The 410-km discontinuity is characterized by  $\sim 4$ –5% increase in the compressional and shear wave velocities in the mantle (e.g. Grand and Helmberger, 1984; Kennett et al., 1995). The olivine to wadsleyite phase transition is widely accepted as the major cause of the 410-km discontinuity. Mao et al. (2008b) reported that the velocity contrast between olivine and wadsleyite at 410-km depth decreases with increasing  $H_2O$  content in wadsleyite, due to the strong reduction in elastic wave velocities in hydrous wadsleyite. However, the discussion in Mao et al. (2008b) was restricted to a comparison between hydrous wadsleyite and anhydrous forsterite. Here, we re-examine the effect of hydration on the velocity contrast at 410-km discontinuity using new experimental data on hydrous forsterite. The calculation is performed at 300 K, and the  $H_2O$  partition coefficient between forsterite and wadsleyite is assumed to be 2 (Frost and Dolejš, 2007).

As discussed above, hydration increases  $V_p$  and  $V_s$  of forsterite at high pressures, and this results in a decrease in the forsterite–wadsleyite velocity contrast at 410-km depth. For a dry mantle, the velocity contrast between forsterite and wadsleyite is 9.1(7)% for compressional waves, and 11.3(10)% for shear waves. For a pyrolite mantle with 60 vol.% olivine, the corresponding velocity contrast would be 5.5(4)% for compressional waves, and 6.8(6)% for shear waves. If the mantle  $H_2O$  content is below saturation, for example, 0.2 wt.%  $H_2O$  in forsterite, and using  $K'_{50}$  and  $G'_0$  of hydrous forsterite determined in this study, the compressional and shear velocity contrasts are decreased to 4.6(4)% and 5.8(4)% respectively. These velocity contrasts are slightly lower than those reported by Mao et al. (2008b). Large shear velocity contrasts of this magnitude are observed in some regional studies (e.g. AU3, Gaherty et al., 1999). With  $\sim 0.4$  wt.%  $H_2O$  in olivine at 410-km depth, the compressional and shear velocity contrasts are further reduced to 3.8(4)% and 4.8(6)%, respectively. These are close to observed values in many regional and global seismic studies. Thus, the velocity contrast between mineralogical modeling and seismic studies could be

reconciled if Earth's mantle contains a on average  $\sim 0.4$  wt.%  $\text{H}_2\text{O}$  in olivine for a pyrolite composition. Regional variations in water content may help explain the variable magnitude of the 410-km discontinuity in

seismic studies. Further measurements on Fe-bearing samples and samples at high temperature will supply additional constraints on the effect of hydration on the velocity contrast at 410-km depth.

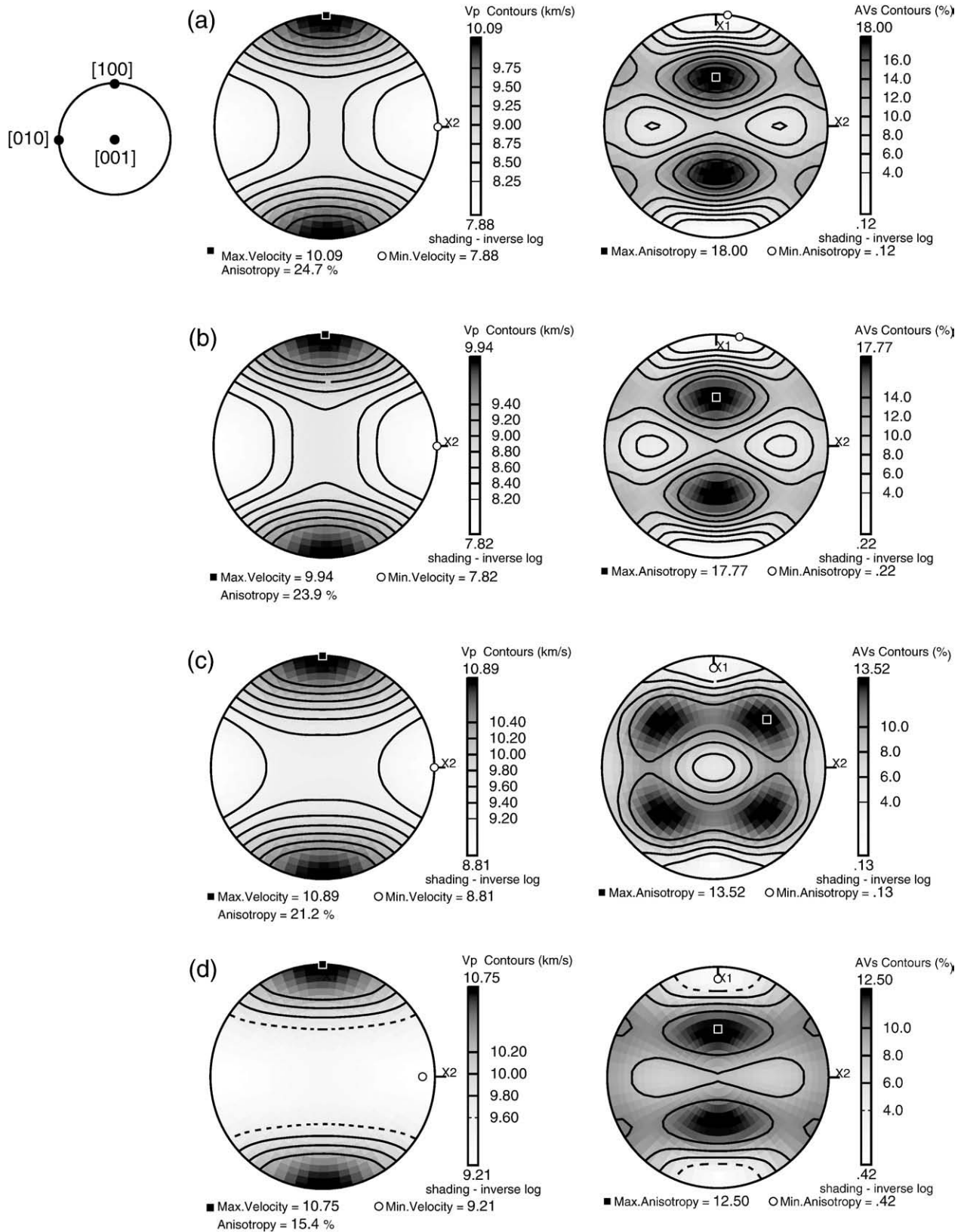


**Fig. 7.** Elastic anisotropy of single-crystal forsterite. Left panels show azimuthal  $V_p$  anisotropy and right panels show shear wave splitting as a function of pressure. (a) Anhydrous forsterite at ambient conditions (Suzuki et al., 1983); (b) hydrous forsterite (0.9 wt.%  $\text{H}_2\text{O}$ ) at ambient conditions (Jacobsen et al., 2008, 2009); (c) anhydrous forsterite at 14.1 GPa (Zha et al., 1996); (d) hydrous forsterite (0.9 wt.%  $\text{H}_2\text{O}$ ) at 14.1 GPa, this study.

#### 4.4. Anisotropy of hydrous forsterite at high pressures

Seismic anisotropy is observed in the upper mantle (e.g. Silver, 1996; Ekström and Dziewonski, 1998), and is believed to be caused by the lattice-preferred orientation (LPO) of minerals (e.g. Mainprice, 2007). For known LPO, the seismic anisotropy can be calculated from the elastic tensor of the constituent single crystals. As the dominant phase in the upper mantle, the behavior of olivine is essential to understand the anisotropic structure of the upper mantle.

Azimuthal anisotropy describes the dependence of velocity on direction of propagation. Fig. 7 shows the azimuthal anisotropy of  $V_p$  for anhydrous and hydrous forsterite single crystals. At ambient conditions, hydration slightly lowers the compressional wave azimuthal anisotropy,  $A_p = (V_{p,max} - V_{p,min})/V_{p,agg}$ , of forsterite from 24.7% to 23.9% (Jacobsen et al., 2008, 2009). With compression, the anisotropy of forsterite is reduced.  $A_p$  of anhydrous forsterite decreases to 21.2% at 14.1 GPa. At the same pressure,  $A_p$  of hydrous forsterite exhibits a stronger decrease from 23.9% to 15.4%. Thus, hydration decreases the compressional wave anisotropy of forsterite at high pressures.

Polarization anisotropy,  $A_s^{po} = (V_{s1} - V_{s2})/V_s$ , is the percentage difference in the velocity of the two shear waves propagating in a given direction. Fig. 7 shows the calculated shear wave splitting of hydrous and anhydrous forsterite. At ambient conditions, the maximum  $A_s^{po}$  of forsterite is the same within uncertainty for hydrous and anhydrous forsterite. At 14.1 GPa, the maximum  $A_s^{po}$  of hydrous forsterite is 12.5%, which is lower than that of anhydrous forsterite (13.5%) at this pressure. Thus, similar to  $A_p$ , the presence of hydrogen modestly decreases the maximum shear wave splitting in forsterite at high pressures.

#### 5. Conclusions

The single-crystal elastic constants of forsterite with 0.9 wt.% H<sub>2</sub>O were measured up to 14.1 GPa at room temperature. Although the bulk and shear moduli of hydrous forsterite are offset to a lower value compared with the anhydrous phase at ambient conditions, they are similar to or greater than those of the anhydrous phase at pressures corresponding to the base of the upper mantle. The addition of 0.9 wt.% H<sub>2</sub>O in forsterite increases the pressure derivatives of the bulk modulus,  $K'_{50}$  from 4.2(2) to 4.50(5) and that of the shear modulus,  $G'_0$  from 1.4(1) to 1.75(5).

Using our experimental results, we investigated the effect of hydration on aggregate sound velocities of forsterite. Although the velocity of hydrous forsterite is slightly lower than that of the anhydrous phase at 1-bar pressure, a velocity crossover occurs around 3–4 GPa. At 410-km depth, incorporation of 0.9 wt.% H<sub>2</sub>O to forsterite increases the compressional and shear wave velocities by 1.1% and 1.9%, respectively. This velocity inversion is consistent with the trend observed for hydrous ringwoodite reported by Jacobsen and Smyth (2006). In addition, hydration decreases the  $V_p/V_s$  ratio of forsterite by 0.7%. At 14.1 GPa, hydration decreases the maximum compressional wave azimuthal anisotropy for single crystals from 21.2% to 15.4%, and the maximum shear wave splitting from 13.5% to 12.5%.

#### Acknowledgments

We thank J. Hu for assistance with X-ray measurements at X17C, NSLS. The petrophysics software used to calculate anisotropy is from David Mainprice. J. R. Smyth and S. D. Jacobsen acknowledge support from the Bayerisches Geoinstitut Visitors Program and the Alexander von Humboldt Foundation for sample synthesis. This research was partially supported by COMPRES, the Consortium for Materials Property Research in Earth Science, Carnegie/DOE alliance center and by NSF grants EAR-0738510 to T. S. Duffy, EAR-0748707 to S. D. Jacobsen and EAR-07-11165 to J. R. Smyth.

#### Appendix A. Supplementary data

Supplementary data associated with this article can be found, in the online version, at doi:10.1016/j.epsl.2010.02.025.

#### References

- Abramson, E.H., Brown, J.M., Slutsky, L.J., Zaug, J., 1997. The elastic constants of San Carlos olivine to 17 GPa. *J. Geophys. Res.* 102, 12,253–12,263.
- Aizawa, Y., Barnhoorn, A., Faul, U.H., Gerald, J.D.F., Jackson, I., Kovács, I., 2008. Seismic properties of Anita Bay dunite: an exploratory study of the influence of water. *J. Petrol.* 49, 841–855.
- Angel, R.J., Bujak, M., Zhao, J., Gatta, G.D., Jacobsen, S.D., 2007. Effective hydrostatic limits of pressure media for high-pressure crystallographic studies. *J. Appl. Crystallogr.* 40, 26–32.
- Bell, D.R., Rossman, G.R., Maldener, J., Endisch, D., Rauch, F., 2003. Hydroxide in olivine: a quantitative determination of the absolute amount and calibration of the IR spectrum. *J. Geophys. Res.* 108, 2150. doi:10.1029/2001JB000679.
- Bercovici, D., Karato, S., 2003. Whole-mantle convection and the transition-zone water filter. *Nature* 425, 39–44.
- Bolfan-Casanova, N., Keppler, H., Rubie, D.C., 2000. Water partitioning between nominally anhydrous minerals in the MgO–SiO<sub>2</sub>–H<sub>2</sub>O system up to 24 GPa: implications for the distribution of water in the Earth's mantle. *Earth Planet. Sci. Lett.* 182, 209–221.
- Brodholt, J., 1997. Ab initio calculations on point defects in forsterite (Mg<sub>2</sub>SiO<sub>4</sub>) and implications for diffusion and creep. *Am. Mineral.* 82, 1049–1053.
- Chopelas, A., 1991. Single crystal Raman spectra of forsterite, fayalite, and monticellite. *Am. Mineral.* 76, 1101–1109.
- Churakov, S.V., Khisina, N.R., Urusov, V.S., Wirth, R., 2003. First-principles study of (MgH<sub>2</sub>SiO<sub>4</sub>)<sub>n</sub>·n(Mg<sub>2</sub>SiO<sub>4</sub>) hydrous olivine structures. 1. Crystal structure modelling of hydrous olivine Hy-2a(MgH<sub>2</sub>SiO<sub>4</sub>)·3(Mg<sub>2</sub>SiO<sub>4</sub>). *Phys. Chem. Mineral.* 30, 1–11.
- Demouchy, S., Deloule, E., Frost, D.J., Keppler, H., 2005. Pressure and temperature-dependence of water solubility in Fe-free wadsleyite. *Am. Mineral.* 90, 1084–1091.
- Dziewonski, A.M., Anderson, D.L., 1981. Preliminary reference earth model. *Phys. Earth Planet. Inter.* 25, 297–356.
- Ekström, G., Dziewonski, A.M., 1998. The unique anisotropy of the Pacific upper mantle. *Nature* 394, 168–172.
- Every, A.G., 1980. General closed-form expressions for acoustic waves in elastically anisotropic solids. *Phys. Rev. B* 22, 1746–1760.
- Frost, D.J., Dolejš, D., 2007. Experimental determination of the effect of H<sub>2</sub>O on the 410-km seismic discontinuity. *Earth Planet. Sci. Lett.* 256, 182–195.
- Gaherty, J.B., Wang, Y.B., Jordan, T.H., Weidner, D.J., 1999. Testing plausible upper-mantle compositions using fine-scale models of the 410-km discontinuity. *Geophys. Res. Lett.* 26, 1641–1644.
- Grand, S.P., Helmberger, D.V., 1984. Upper mantle shear structure of North America. *Geophys. J. R. Astron. Soc.* 76, 399–438.
- Hauri, E.H., Gaetani, G.A., Green, T.H., 2006. Partitioning of water during melting of the Earth's upper mantle at H<sub>2</sub>O-undersaturated conditions. *Earth Planet. Sci. Lett.* 248, 715–734.
- Hirschmann, M.M., 2006. Water, melting, and the deep earth H<sub>2</sub>O cycle. *Annu. Rev. Earth Planet. Sci.* 34, 629–653.
- Hirschmann, M.M., Aubaud, C., Withers, A.C., 2005. Storage capacity of H<sub>2</sub>O in nominally anhydrous minerals in the upper mantle. *Earth Planet. Sci. Lett.* 236, 167–181.
- Holl, C.M., Smyth, J.R., Jacobsen, S.D., Frost, D.J., 2008. Effects of hydration on the structure and compressibility of wadsleyite, β-(Mg<sub>2</sub>SiO<sub>4</sub>). *Am. Mineral.* 93, 598–607.
- Huang, X.G., Xu, Y.S., Karato, S., 2005. Water content in the transition zone from electrical conductivity of wadsleyite and ringwoodite. *Nature* 434, 746–749.
- Hushur, A., Manghnani, M.H., Smyth, J.R., Nestola, F., Frost, D.J., 2009. Crystal chemistry of hydrous forsterite and its vibrational properties up to 41 GPa. *Am. Mineral.* 94, 751–760.
- Inoue, T., 1994. Effect of water on melting phase relations and melt composition in the system Mg<sub>2</sub>SiO<sub>4</sub>–MgSiO<sub>3</sub>–H<sub>2</sub>O up to 15 GPa. *Phys. Earth Planet. Inter.* 85, 237–263.
- Inoue, T., Weidner, D.J., Northrup, P.A., Parise, J.B., 1998. Elastic properties of hydrous ringwoodite (γ-phase) in Mg<sub>2</sub>SiO<sub>4</sub>. *Earth Planet. Sci. Lett.* 160, 107–113.
- Isaak, D.G., Anderson, O.L., Goto, T., Suzuki, I., 1989. Elasticity of single-crystal forsterite measured to 1700 K. *J. Geophys. Res.* 94, 5895–5906.
- Jackson, I., Gerald, J.D.F., Faul, U.H., Tan, B.H., 2002. Grain-size-sensitive seismic wave attenuation in polycrystalline olivine. *J. Geophys. Res.* 107, 2360.
- Jacobsen, S.D., 2006. Effect of water on the equation of state of nominally anhydrous minerals. In: Keppler, H., Smyth, J.R. (Eds.), *Water in Nominally Anhydrous Minerals, Reviews in Mineralogy and Geochemistry: Mineralogical Society of America, Chantilly, Virginia*, vol. 62, pp. 321–342.
- Jacobsen, S.D., Jiang, F., Mao, Z., Duffy, T.S., Smyth, J.R., Holl, C.M., Frost, D.J., 2008. Effects of hydration on the elastic properties of olivine. *Geophys. Res. Lett.* 35, L14303.
- Jacobsen, S.D., Jiang, F., Mao, Z., Duffy, T.S., Smyth, J.R., Holl, C.M., Frost, D.J., 2009. Correction to effects of hydration on the elastic properties of olivine. *Geophys. Res. Lett.* 36, L12302. doi:10.1029/2009GL038660.
- Jacobsen, S.D., Smyth, J.R., 2006. Effect of water on the sound velocities of ringwoodite in the transition zone. In: Jacobsen, S.D., van der Lee, S. (Eds.), *Earth's Deep Water Cycle. American Geophysical Union, Washington, D. C.*, pp. 131–145.
- Jacobsen, S.D., Smyth, J.R., Spetzler, H., Holl, C.M., Frost, D.J., 2004. Sound velocities and elastic constants of iron-bearing hydrous ringwoodite. *Phys. Earth Planet. Inter.* 143–144, 47–56.

- Jacobsen, S.D., van der Lee, S. (Eds.), 2006. Earth's Deep Water Cycle. American Geophysical Union, Washington, D. C. p. 313.
- Karato, S., 1993. Importance of anelasticity in the interpretation of seismic tomography. *Geophys. Res. Lett.* 20, 1623–1626.
- Karato, S., 1995. Effects of water on seismic wave velocities in the upper mantle. *Proc. Jpn Acad.* 71, 61–66.
- Karato, S., Paterson, M.S., Fitzgerald, J.D., 1986. Rheology of synthetic olivine aggregates: influence of grain size and water. *J. Geophys. Res.* 91, 8151–8176.
- Kennett, B.L.N., Engdahl, E.R., Buland, R., 1995. Constraints on seismic velocities in the Earth from travel-times. *Geophys. J. Int.* 122, 108–124.
- Kleppe, A.K., Jephcoat, A.P., 2006. Raman spectroscopic studies of hydrous and nominally anhydrous deep mantle phases. In: Jacobsen, S.D., van der Lee, S. (Eds.), *Earth's Deep Water Cycle*. American Geophysical Union, Washington, D. C., pp. 69–93.
- Kohlstedt, D.L., Keppler, H., Rubie, D.C., 1996. Solubility of water in the  $\alpha$ ,  $\beta$  and  $\gamma$  phases of  $(\text{Mg}, \text{Fe})_2\text{SiO}_4$ . *Contrib. Mineral. Petrol.* 123, 345–357.
- Kudoh, Y., 2008. Crystal structural features of hydrous forsterite: effect of Fe on the M-site vacancies, possible hydrogen positions and variation of the unit cell dimensions. *J. Mineral. Petrol. Sci.* 103, 371–375.
- Li, B., 2003. Compressional and shear wave velocities of ringwoodite  $\gamma$ - $\text{Mg}_2\text{SiO}_4$  to 12 GPa. *Am. Mineral.* 88, 1312–1317.
- Liu, L., Du, J., Zhao, J., Liu, H., Gao, H., Chen, Y., 2009. Elastic properties of hydrous forsterites under high pressure: first-principle calculations. *Phys. Earth Planet. Inter.* 176, 89–97.
- Mainprice, D., 2007. Seismic anisotropy of the deep Earth from a mineral and rock physics perspective. In: Schubert, G. (Ed.), *Treatise on Geophysics*, Vol. 2. Elsevier Ltd, Oxford, pp. 437–492.
- Manthilake, M.A.G.M., Matsuzaki, T., Yoshino, T., Yamashita, S., Ito, E., Katsura, T., 2009. Electrical conductivity of wadsleyite as a function of temperature and water content. *Phys. Earth Planet. Inter.* 174, 10–18.
- Mao, Z., Jacobsen, S.D., Jiang, F., Smyth, J.R., Holl, C., Frost, D.J., Duffy, T.S., 2008a. Single-crystal elasticity of wadsleyites,  $\beta$ - $\text{Mg}_2\text{SiO}_4$ , containing 0.37–1.66 wt%  $\text{H}_2\text{O}$ . *Earth Planet. Sci. Lett.* 268, 540–549.
- Mao, Z., Jacobsen, S.D., Jiang, F., Smyth, J.R., Holl, C.M., Duffy, T.S., 2008b. Elasticity of hydrous wadsleyite to 12 GPa: implications for Earth's transition zone. *Geophys. Res. Lett.* 35, L21305. doi:10.1029/2008GL035618.
- Mei, S., Kohlstedt, D.L., 2000a. Influence of water on plastic deformation of olivine aggregates 1. Diffusion creep regime. *J. Geophys. Res.* 105, 21,457–21,469.
- Mei, S., Kohlstedt, D.L., 2000b. Influence of water on plastic deformation of olivine aggregates 2. Dislocation creep regime. *J. Geophys. Res.* 105, 21,471–21,481.
- Mosenfelder, J.L., Deligne, N.I., Asimow, P.D., Rossman, G.R., 2006. Hydrogen incorporation in olivine from 2–12 GPa. *Am. Mineral.* 91, 285–294.
- Nolet, G., Zielhuis, A., 1994. Low S velocities under the Tornquist–Teisseyre zone: evidence for water injection into the transition zone by subduction. *Geophys. Res. Lett.* 99, 15,813–15,820.
- Shimizu, H., 1995. High-pressure Brillouin scattering of molecular single-crystals grown in a diamond-anvil cell. In: Senoo, M., Suito, K., Kobayashi, T., Kubota, H. (Eds.), *High Pressure Research on Solids*. Elsevier, Netherlands, pp. 1–17.
- Silver, P.G., 1996. Seismic anisotropy beneath the continents: probing the depths of geology. *Annu. Rev. Earth Planet. Sci.* 24, 385–432.
- Sinogeikin, S.V., Bass, J.D., 2000. Single-crystal elasticity of pyrope and  $\text{MgO}$  to 20 GPa by Brillouin scattering in the diamond cell. *Phys. Earth Planet. Inter.* 120, 43–62.
- Sinogeikin, S.V., Bass, J.D., Katsura, T., 2001. Single-crystal elasticity of  $\gamma$ - $(\text{Mg}_{0.91}\text{Fe}_{0.09})_2\text{SiO}_4$  to high pressures and to high temperatures. *Geophys. Res. Lett.* 28, 4335–4338.
- Sinogeikin, S.V., Bass, J.D., Katsura, T., 2003. Single-crystal elasticity of ringwoodite to high pressures and high temperatures: implications for 520 km seismic discontinuity. *Phys. Earth Planet. Inter.* 136, 41–66.
- Smyth, J.R., 1987.  $\beta$ - $\text{Mg}_2\text{SiO}_4$ : a potential host for water in the mantle? *Am. Mineral.* 72, 1051–1055.
- Smyth, J.R., Frost, D.J., Nestola, F., Holl, C.M., Bromiley, G., 2006. Olivine hydration in the deep upper mantle: effects of temperature and silica activity. *Geophys. Res. Lett.* 33, L15301. doi:10.1029/2006GL026194.
- Song, T.A., Helmberger, D.V., Grand, S.P., 2004. Low-velocity zone atop the 410-km seismic discontinuity in the northwestern United States. *Nature* 427, 530–533.
- Speziale, S., Duffy, T.S., 2002. Single-crystal elastic constants of fluorite ( $\text{CaF}_2$ ) to 9.3 GPa. *Phys. Chem. Mineral.* 29, 465–475.
- Speziale, S., Duffy, T.S., Angel, R.J., 2004. Single-crystal elasticity of fayalite to 12 GPa. *J. Geophys. Res.* 109, B12202.
- Suzuki, I., Anderson, O.L., Sumino, Y., 1983. Elastic properties of a single-crystal forsterite  $\text{Mg}_2\text{SiO}_4$ , up to 1, 200 K. *Phys. Chem. Mineral.* 10, 38–46.
- Tseng, T.L., Chen, W.P., 2008. Discordant contrasts of P- and S-wave speeds across the 660-km discontinuity beneath Tibet: a case for hydrous remnant of sub-continental lithosphere. *Earth Planet. Sci. Lett.* 268, 450–462.
- Tsuchiya, J., Tsuchiya, T., 2009. First principles investigation of the structural and elastic properties of hydrous wadsleyite under pressure. *J. Geophys. Res.* 114, B02206. doi:10.1029/2008JB005841.
- van der Lee, S., Regenauer-Lieb, K., Yuen, D.A., 2008. The role of water in connecting past and future episodes of subduction. *Earth Planet. Sci. Lett.* 273, 15–27.
- van der Meijde, M., Marone, F., Giardini, D., van der Lee, S., 2003. Seismic evidence for water deep in Earth's upper mantle. *Science* 300, 1556–1558.
- Vinnik, L., Farra, V., 2007. Low s velocity atop the 410-km discontinuity and mantle plumes. *Earth Planet. Sci. Lett.* 262, 398–412.
- Wang, J., Sinogeikin, S.V., Inoue, T., Bass, J.D., 2003. Elastic properties of hydrous ringwoodite. *Am. Mineral.* 88, 1608–1611.
- Wang, J., Sinogeikin, S.V., Inoue, T., Bass, J.D., 2006. Elastic properties of hydrous ringwoodite at high-pressure conditions. *Geophys. Res. Lett.* 33, L14308. doi:10.1029/2006GL026441.
- Yoshino, T., Manthilake, G., Matsuzaki, T., Katsura, T., 2008. Dry mantle transition zone inferred from the conductivity of wadsleyite and ringwoodite. *Nature* 451, 326–329.
- Zha, C.S., Duffy, T.S., Downs, R.T., Mao, H.K., Hemley, R.J., 1996. Sound velocity and elasticity of single-crystal forsterite to 16 GPa. *J. Geophys. Res.* 101, 17,535–17,545.